Talanta 279 (2024) 126587

Contents lists available at ScienceDirect

Talanta

journal homepage: www.elsevier.com/locate/talanta

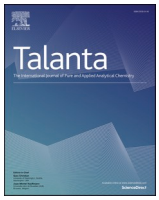

Near-infrared fluorescent probe for ultrasensitive detection of organophosphorus pesticides and visualization of their interaction with butyrylcholinesterase in living cells

Zhimin Zhang [a], Jingkang Li [a], Bin Yang [a], Mo Ma [a,b], Xiangdong Ding [c], Hui Shi [a], Pinyi Ma [a], Daqian Song [a], Ziwei Zhang [a,*]

[a] College of Chemistry, Jilin Province Research Center for Engineering and Technology of Spectral Analytical Instruments, Jilin University, Qianjin Street 2699, Changchun, 130012, China
[b] School of Pharmacy, Jilin University, Qianjin Street 2699, Changchun, 130012, China
[c] China-Japan Union Hospital, Jilin University, Xiantai Street 126, Changchun, 130012, China

ARTICLE INFO

Keywords:
Butyrylcholinesterase
Organophosphorus pesticides
Near-infrared fluorescent probe
Oxon pesticide
Thion pesticide

ABSTRACT

The toxicity of organophosphorus pesticides (OPs) can catastrophically cause liver cell damage and inhibit the catalytic activity of cholinesterase. We designed and synthesized a near-infrared fluorescent probe HP-LZB with large Stokes shift which can specifically identify and detect butyrylcholinesterase (BChE) and visually explore the interaction between OPs and endogenous BChE in living cells. Fluorescence was turned on when HP-LZB was hydrolyzed into HP-LZ in the presence of BChE, and OPs could inhibit BChE's activity resulting in a decrease of fluorescence. Six OPs including three oxon pesticides (paraoxon, chlorpyrifos oxon and diazoxon) and their corresponding thion pesticides (parathion, chlorpyrifos and diazinon) were investigated. Both in vitro and cell experiments indicated that only oxon pesticides could inhibit BChE's activity. The limits of detection (LODs) of paraoxon, chlorpyrifos oxon and diazoxon were as low as 0.295, 0.007 and 0.011 ng mL^{-1} respectively and the recovery of OPs residue in vegetable samples was satisfactory. Thion pesticides themselves could hardly inhibit the activity of BChE and are only toxic when they are converted to their corresponding oxon form in the metabolic process. However, in this work, thion pesticides were found not be oxidized into their oxon forms in living HepG2 cells due to the lack of cytochrome P450 in hepatoma HepG2 cell lines. Therefore, this probe has great application potential in effectively monitoring OPs in real plant samples and visually exploring the interaction between OPs and BChE in living cells.

1. Introduction

The use of pesticides is essential for crop production in modern agriculture. However, overuse of pesticides can lead to environmental pollution including pollution of water, rivers and soil. Over time, pesticides and their metabolites may accumulate in humans and animals through surface water flow, groundwater infiltration and other pathways [1–3]. Therefore, in addition to the need to detect pesticides in the environment, it is also crucial to monitor the accumulation of pesticides in biological samples.

Organophosphorus pesticides (OPs) have always occupied an important position in pesticides because of their high efficiency in pest control and rapid biodegradation [4,5]. However, the residues of these pesticides pose a potential threat to the environment and even human health. OPs inhibit the activity of cholinesterase and cause a series of neurological diseases and even death [6]. So far, some traditional methods for detecting OPs are widely applied, including liquid chromatography [7], mass spectrometry [8] and gas chromatography/mass spectrometry (GC/MS) [9]. However, so far, most studies were carried out on environmental or vegetable and fruit samples, and only a few researchers have visually detected OPs in living cells [10]. As the harm of pesticides becomes more and more serious, it is urgent to deeply understand the harm mechanism of different OPs through visual imaging in living cells.

BChE has detoxification effect and can degrade and detoxify a variety of organophosphorus compounds, including certain pesticides and nerve

* Corresponding author.
E-mail address: zzw@jlu.edu.cn (Z. Zhang).

https://doi.org/10.1016/j.talanta.2024.126587
Received 7 April 2024; Received in revised form 19 June 2024; Accepted 17 July 2024
Available online 18 July 2024

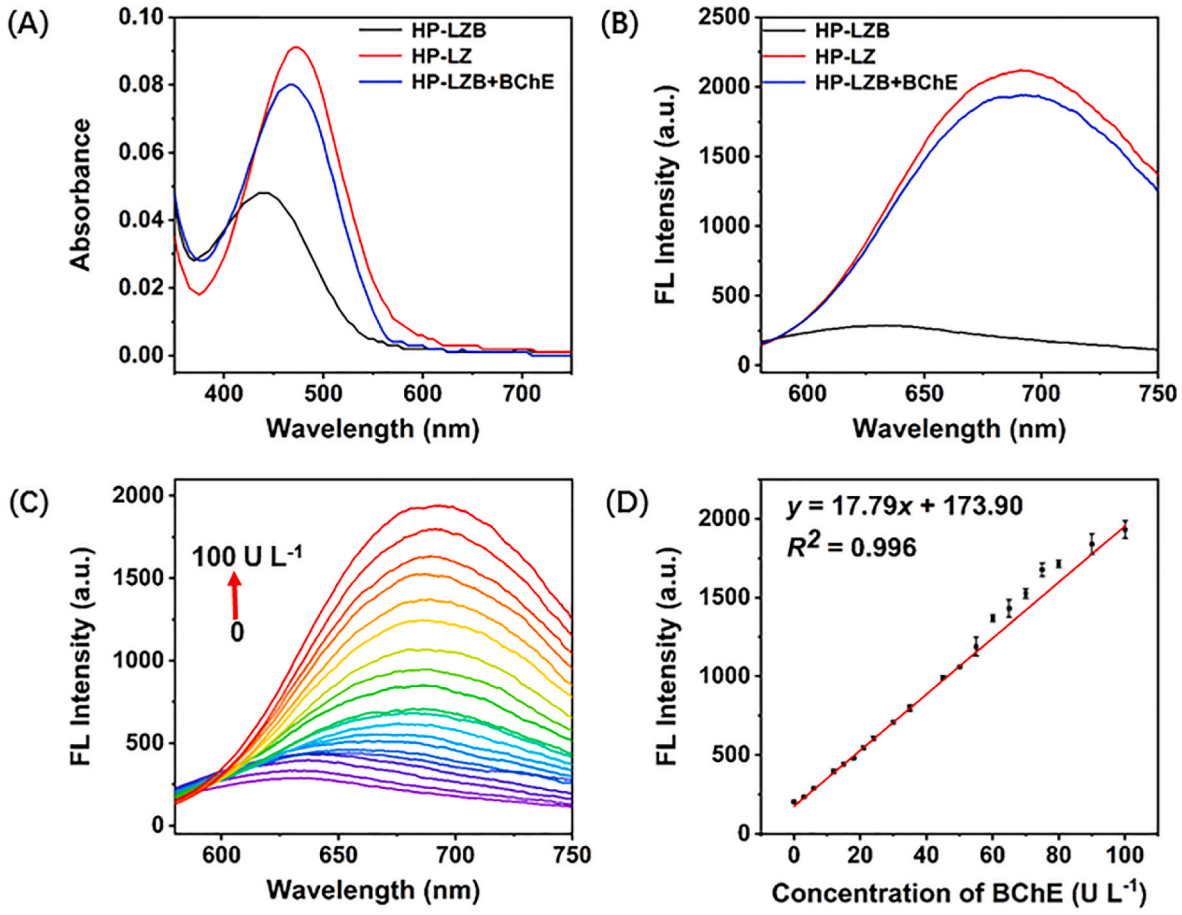

Fig. 1. UV–vis (A) and fluorescent (B) spectra of 10 μmol L^{-1} HP-LZ and HP-LZB in the absence and presence of BChE. (C) Fluorescent spectra for samples with BChE at different concentrations from 0 to 100 U L^{-1}. (D) Linear fitting diagram of fluorescence intensity and BChE concentration. BChE concentrations range from 0 to 100 U L^{-1}. The error bar represents SD ($n = 3$). All measurements were performed at 37 °C in 10 mmol L^{-1} PBS. Wavelengths of excitation (λex) and emission (λem) were 520 nm and 690 nm, respectively.

agents [11–13]. Some publications have reported the detection of OPs utilizing their inhibition effects on BChE. Some of them used nanomaterials as the probe [6,14,15] and a few of them used organic small molecule fluorophore as the probe [16,17]. In this work, for the first time, the inhibition of BChE by OPs was visually observed in living cells under microscope and the interaction between oxon/thion OPs and endogenous BChE in cells were better understood.

Herein, in order to further elucidate the toxicity of pesticides at the cellular level, we designed a large Stokes shift fluorescent probe HP-LZB based on the principle of intramolecular charge transfer (ICT) which emits fluorescent signal in the near-infrared spectral range after interaction with BChE [18]. With this probe, BChE levels in vitro can be quantitatively determined and those in living cells can be qualitatively visualized. We applied this probe to the detection of OPs both in vitro and in living cells. The toxicity of three pairs of oxon pesticides and their thion forms were differentiated when interacting with BChE in hepatoma cells. The developed probe has not only high sensitivity and selectivity, but also good stability and biocompatibility, and has great potential in pesticide residue monitoring.

2. Materials and methods

2.1. Synthesis of the probe HP-LZB

The synthetic route of HP-LZB was depicted in Scheme S1. The chemical structures of the intermediates and the product were confirmed by nuclear magnetic resonance (NMR) and mass spectroscopy (MS). The NMR spectra are displayed in Figures S1 to S6, and the MS spectra are displayed in Figure S7 to S10.

2.2. Fluorescent measurement

All spectra were recorded in 1 mL buffer composed of PBS (10 mmol L^{-1}, pH 7.4) and DMSO in a ratio of 95:5 (v/v). In each sample, there were 10 μL of 1 mmol L^{-1} HP-LZB and different concentrations of BChE. After 60 min shaking at 37 °C, the fluorescent spectrum was collected for each sample. The spectra were recorded at 37 °C on a Hitachi F-7000 fluorescence spectrometer with $\lambda ex = 520$ nm and $\lambda em = 690$ nm. All the experiments were performed in triplicate.

2.3. Detection of OPs

Distilled water was used to dilute each OP to the desired concentration. 100 μL different concentrations of OP were incubated with 100 μL BChE for 30 min at 37 °C in an oscillator. Then the mixture was mixed with 10 μL HP-LZB, 40 μL DMSO and 750 μL PBS for 60 min at 37 °C. In the resulting solution, the concentrations of BChE and HP-LZB were respectively 60 U L^{-1} and 10 μmol L^{-1}. The fluorescence spectrum for the resulting solution was recorded at 37 °C.

4 g of Chinese cabbage leaves was gathered and mashed. 4 mL of methanol was mixed with the mashed leaves. The mixture was ultrasonic treated for 30 min, centrifuged at 6000 rpm for 10 min, and filtered through a membrane filter with a pore size of 0.22 μm. The cabbage extract was spiked with different concentrations of paraoxon

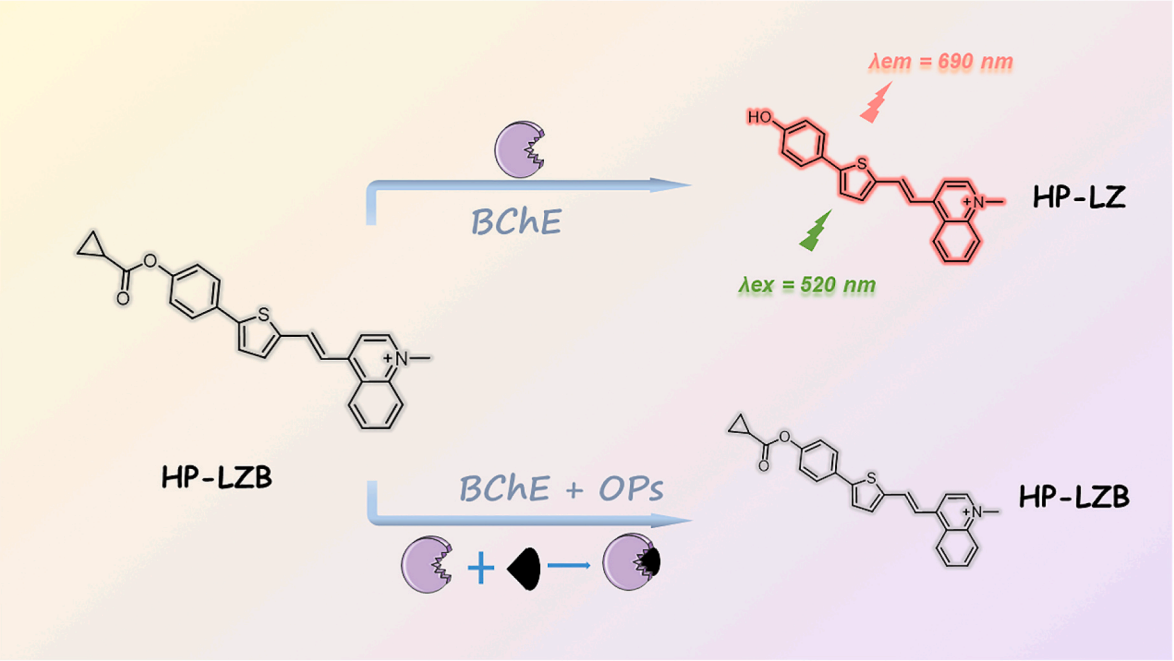

Fig. 2. Recognition mechanism of probe HP-LZB for detection of BChE and OPs.

and then the fluorescence of the sample was measured.

2.4. Experimental procedures for cell imaging

HepG2 cells were cultured in DMEM medium supplemented with 10 % fetal bovine serum (FBS) and 1 % penicillin and streptomycin in a 5 % CO_2 incubator at 37 °C. The cells were inoculated into a cell culture Petri dish with a diameter of 35 mm and incubated in 1 mL of medium for 24 h before the cell imaging. Cell imaging experiments were carried out on an Olympus IX-73 inverted microscope equipped with a DP72 camera. For fluorescence imaging, the excitation wavelength was 510–550 nm and the emission wavelength was >590 nm. The cell fluorescent intensity was measured using software ImageJ and the significant statistical differences were analyzed using software GraphPad Prism 9.

2.5. Experimental procedures for in vivo imaging

The experiment followed the ethical regulations of Institutional Animal Care and Use Committee of Jilin University (permit number SY202306031). A male C57BL/6J mouse aged 4–5 weeks was injected with 100 μL of 200 μmol L^{-1} HP-LZB, and the fluorescence imaging was collected respectively at 0, 10, 20, 30, 40, 50 and 60 min. The *in vivo* imaging experiments were conducted on the IVIS Lumina LT Series III small animal imaging system using an excitation wavelength of 500 nm and a filter of 700 nm.

3. Results and discussion

3.1. Characterization of HP-LZB

The UV–vis spectra of HP-LZ and HP-LZB in the presence of BChE are shown in Fig. 1A and 520 nm was selected as the excitation wavelength. When excited at 520 nm the fluorescence difference between HP-LZ and HP-LZB was largest. The fluorescent spectra of HP-LZ and HP-LZB in the presence of BChE are shown in Figs. 1B and 690 nm was selected as the emission wavelength. As seen in Fig. 1B, the probe HP-LZB gives very weak fluorescent signal whereas BChE's hydrolysis product HP-LZ shows a strong fluorescence. The absolute fluorescence quantum yield of HP-LZ was measured on an Edinburgh FLS 920 fluorescence spectrometer and determined as 5.0 %.

3.2. Sensing mechanism for BChE detection

As seen in Fig. 2, under the catalysis of BChE, the probe HP-LZB which has almost no fluorescent signal is hydrolyzed to HP-LZ with a good fluorescent signal. BChE specifically recognizes and cleaves the cyclopropyl carbonyl group in HP-LZB [19]. High performance liquid chromatography (HPLC) was applied to prove the mechanism of the enzyme digestion reaction and the results in Figure S11 show chromatograms obtained with HP-LZB, HP-LZ and the mixture of HP-LZB and BChE. Two chromatographic peaks are observed in the chromatogram for the mixture of HP-LZB and BChE. The retention time of the two peaks is consistent with that of HP-LZB and HP-LZ, as proves the occurrence of the enzymatic reaction. In order to further confirm the occurrence of the enzymatic reaction, the mass spectroscopy spectrum for the mixture of HP-LZB and BChE was recorded and shown in Figure S12. The two peaks in the MS spectrum with *m/z* values of 412.1 and 344.1 attribute respectivly to HP-LZB and HP-LZ, as confirms the hydrolysis of HP-LZB to HP-LZ by BChE.

3.3. Optimization of experimental conditions

In order to obtain the best fluorescent signal, two experimental conditions, including the pH and the incubation time during the reaction of probe HP-LZB and BChE, were optimized. As seen in Figure S13, in the presence of 55 U L^{-1} BChE, the signal intensity reaches the maximum at pH 7.0. The physiological pH (7.4) was selected as the pH of the reaction solution in the following experiments because at pH 7.4 the physiological compatibility is high and the physiological functions of the cells will not be affected. The change of fluorescent intensity with the incubation time in the presence of 100 U L^{-1} BChE is shown in Figure S14. After more than 60 min, the signal almost reached a plateau, so the incubation time of the reaction was set at 60 min. The stability of both HP-LZ and HP-LZB under light irradiation at 520 nm was tested, and the results in Figure S15 indicate that the fluorescent intensity of both HP-LZ and HP-LZB is quite stable within a period of 1 h.

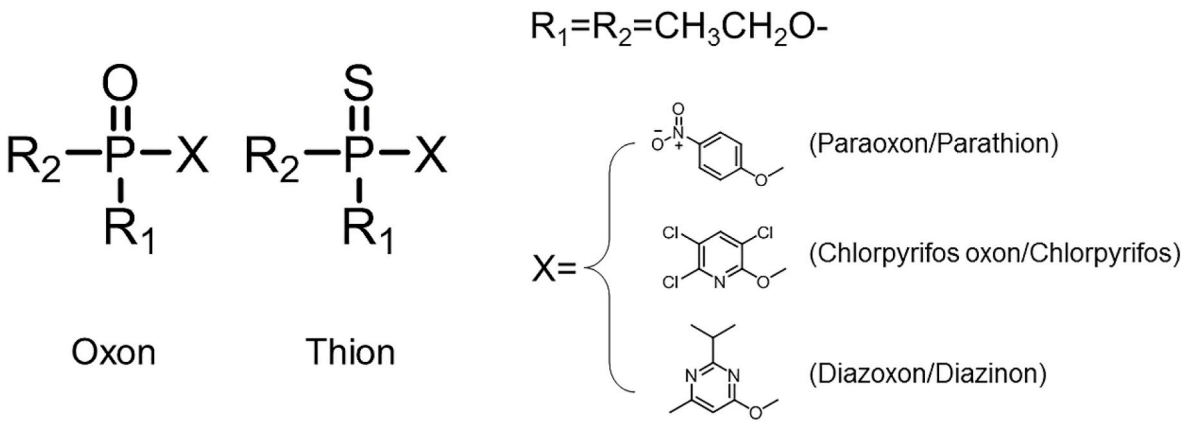

Fig. 3. Structure diagram of three oxon pesticides and three thion pesticides.

3.4. Detection of BChE in vitro

The fluorescent spectra for samples with BChE at concentrations between 0 and 100 U L^{-1} in the presence of 10 μmol L^{-1} HP-LZB are displayed in Fig. 1C. The standard curve (fluorescent intensity vs. BChE concentration) is plotted in Fig. 1D. The linear part of the curve between 0 and 100 U L^{-1} is well simulated using a linear function which is FL intensity = 17.8 (±0.3) [BChE] + 173.9 (±8.0). The linear correlation coefficient r is 0.998. The limit of detection (LOD) for BChE which was calculated based on 3SD/slope (n = 7) is 0.896 U L^{-1}.

The analytical performance of some fluorescent probes for detecting BChE is summarized in a previous publication including λex, λem and LOD [20]. For HP-LZ, λex and λem are respectively 520 and 690 nm. It is a near-infrared probe and emits light of 690 nm which allows for deeper penetration in biological tissues than visible light during imaging [21]. Moreover, the emission wavelength has a large Stokes shift up to 170 nm and such a large Stokes shift leads to a higher signal-to-background ratio in fluorescent imaging [22]. Considering that the LODs of fluorescent probes in the literature ranges from 0.04 to 80 U L^{-1}, the LOD of the present method (0.896 U L^{-1}) is low enough, indicating a good affinity between HP-LZB and BChE [20].

The reaction kinetics between HP-LZB and BChE was investigated and the Michaelis-Menten curve is shown in Figure S16. The linear fit of the Lineweaver-Burk plot in Figure S17 gives a maximum reaction velocity (V_{max}) of 0.57 μmol L^{-1} min^{-1} and a Michaelis-Menten constant (K_m) of 3.07 μmol L^{-1} which is lower than K_m of BChE with acetylcholine as the substrate [23]. These results indicate that HP-LZB has a high affinity towards BChE.

Figure S18 shows that the fluorescence responses of HP-LZB to 54 kinds of substances commonly existing in biological organism including BChE's analogue acetylcholinesterase (AChE) were neglectable. The results indicate that the proposed method has very good anti-interference capability and is suitable to the determination of BChE in complex matrix samples.

3.5. Mechanism for the inhibition of BChE by OPs

All OP molecules contain a phosphorus atom that forms either a P═O bond or a P═S bond. The compounds with a P═O bond are classified as oxon pesticides, while those with a P═S bond are categorized as thion pesticides [24]. The molecular structures for the three oxon pesticides and three thion pesticides studied in this work are displayed in Fig. 3.

Thion pesticides themselves could hardly inhibit the activity of BChE. They are converted into their corresponding oxon forms in the process of human or animal metabolism, e.g. parathion would be transformed into paraoxon during the metabolism [25]. Such conversion increases the toxicity of thion pesticide and enhances its anti-cholinesterase efficacy [25,26].

Oxon pesticide could effectively inhibit the catalytic activity of BChE by phosphorylation of the serine residue in the active site of the enzyme. As shown in Fig. 2, with more oxon pesticide in the sample, more effectively BChE is inhibited with less HP-LZB hydrolyzed to HP-LZ, and subsequently less fluorescence is emitted. Thus the fluorescent signal is inversely proportional to oxon pesticide's concentration and can be used to evaluate the level of oxon pesticide in the sample.

All three oxon pesticides studied in this work have a common diethyl phosphate moiety (see Fig. 3). It has been demonstrated that the binding affinity between organophosphorus pesticide and BChE increases proportionally with alkyl chain length and diethyl phosphate pesticide exhibits a significantly lower inhibition constant compared to dimethyl phosphate [27]. Thus the three oxon pesticides with common diethyl phosphate structure should have strong interaction with BChE and can effectively suppress its activity.

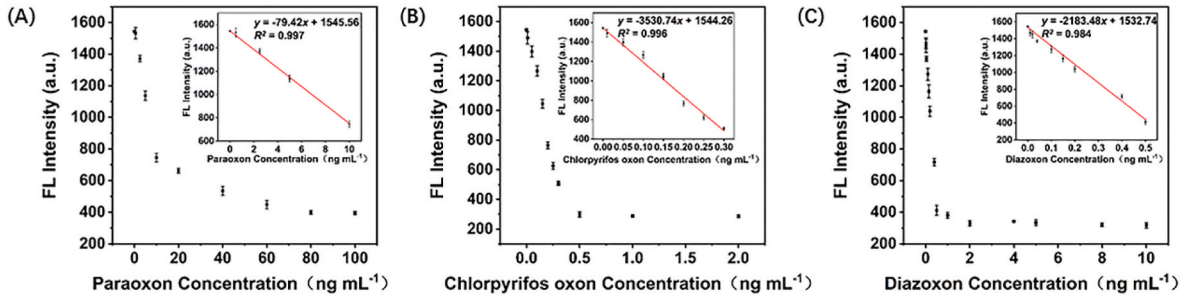

Fig. 4. Plots of fluorescence intensity vs. concentration of pesticides including (A) paraoxon, (B) chlorpyrifos oxon, (C) diazoxon. The concentration of BChE was 60 U L^{-1}. Inset shows the linear fit part. The error bar represents SD (n = 3).

Table 1
Detection of spiked paraoxon in the extracts of three kinds of vegetable leaves.

Vegetable	Spike (ng mL^{-1})	Found (ng mL^{-1})	Recovery (%)	RSD (%, n = 3)
Chinese cabbage	4.0	4.3 ± 0.1	107	3.1
	8.0	8.3 ± 0.4	104	5.2
oilseed rape	4.0	4.3 ± 0.3	107	6.3
	8.0	8.6 ± 0.4	108	4.5
pak choi	4.0	4.3 ± 0.2	106	4.7
	8.0	8.5 ± 0.1	106	0.7

3.6. Detection of organophosphorus pesticides

In order to testify the practicability of probe HP-LZB for the detection of OPs, six OPs were determined by the present method. When BChE's activity is inhibited by OP, less HP-LZB is hydrolyzed to HP-LZ and thus the fluorescent intensity is inversely proportional to OP's concentration. The standard curves (fluorescent intensity vs. OP's concentration) for the six OPs are shown in Fig. 4 and Figure S19.

As seen in Fig. 4, for the three oxon pesticides (paraoxon, chlorpyrifos oxon and diazoxon), with the increase of OP's concentration, the fluorescent intensity first goes down linearly and then decreases slowly until reaching a platform. The linear part of the curves is well fitted by the linear equations with the correlation coefficients ranging from 0.992 to 0.999 (see the inset graphs in Fig. 4). The regression equations for paraoxon, chlorpyrifos oxon and diazoxon are respectively FL intensity = −79 ± 2 [Paraoxon] + 1545 ± 4, FL intensity = −3530 ± 83 [Chlorpyrifos Oxon] + 1544 ± 9 and FL intensity = −2183 ± 106 [Diazoxon] + 1532 ± 12. The LODs (3SD/slope with $n = 7$) for detecting paraoxon, chlorpyrifos oxon and diazoxon are respectively 0.295, 0.007 and 0.011 ng mL^{-1}. At the same concentration, chlorpyrifos oxon and diazoxon are found to have much higher toxicity to BChE than paraoxon. The activity of BChE is almost completely inhibited by chlorpyrifos oxon and diazoxon at very low concentration.

In Table S1, the LOD and linear range of the three oxon pesticides obtained by the present method are compared with those obtained by the reported methods. The LODs for the oxon pesticides (0.007–0.295 ng mL^{-1}) are low enough especially for chlorpyrifos oxon (0.007 ng mL^{-1}) and diazoxon (0.011 ng mL^{-1}). Such low LODs indicated that the proposed fluorescent probe is very sensitive when detecting oxon OPs.

The analytical performance was further compared with the reported fluorescent probe [16]. In the reference, two pesticides (*iso*-OMPA and DDVP) were detected: the linear range for detecting *iso*-OMPA is 1.0 × 10^{-8}-1.0 × 10^{-4} M, and that for detecting DDVP is 1.0 × 10^{-8}-1.0 × 10^{-5} M. As shown in Table S1, the linear range for detecting paraoxon corresponds to 3.6 × 10^{-9}-3.6 × 10^{-8} M, that for detecting chlorpyrifos oxon corresponds to 8.0 × 10^{-11}-1.1 × 10^{-9} M, and that for detecting diazoxon corresponds to 1.3 × 10^{-10}-1.8 × 10^{-9} M. Compared with the reference, the probe proposed in the reference has a wider linear range, whereas the probe in this work has lower LODs.

However as seen in Figure S19, when the three thion pesticides (parathion, chlorpyrifos and diazinon) were used, the fluorescent intensity did not obviously decrease even at a high concentration. Such result confirms that thion pesticides themselves could hardly inhibit the activity of BChE and are only toxic when they are converted to their corresponding oxon forms.

3.7. Detection of paraoxon in Chinese cabbage

The extracts of the leaves from three kinds of vegetables including Chinese cabbage, oilseed rape and pak choi were measured to have no effect on the signal and used as the negative control. The extract was diluted and spiked with different concentrations of paraoxon. The spiked sample was first mixed with BChE and then with HP-LZB. The resulting analytical samples were analyzed by fluorescence spectrometry. As shown in Table 1, the recoveries of paraoxon at 4.0 and 8.0 ng mL^{-1} in spiked vegetable extract samples are between 104 % and 108 %. The accuracy of the present method was further verified by comparison with High Performance Liquid Chromatography (HPLC) method. When different concentrations of paraoxon were spiked into the oilseed rape extract, the concentrations of paraoxon determined by HPLC were 39.8 and 80.1 ng mL^{-1}, and those determined by the present method were 42.9 and 86.2 ng mL^{-1}. The consistence between the present method and HPLC indicates the accuracy of the present method.

3.8. Cell imaging of BChE

Before applying HP-LZB to visual observation of living cells, its toxic effects on HepG2 cells were determined using the CCK-8 kit. The results are shown in Figure S20 and the survival rate of HepG2 cells incubated with 10 μmol L^{-1} HP-LZB was close to 95 %. Due to its low cytotoxicity and excellent in vitro fluorescence response to BChE, HP-LZB will be further used for fluorescence imaging and detection of BChE in living cells.

The targeting ability of HP-LZB to intracellular BChE was demonstrated. The change of the fluorescence brightness of HepG2 cells over time from 0 to 60 min after the addition of HP-LZB was studied in Figure S21. It is found that with the passage of time, the probe approximately reaches the highest brightness level after 40 min of incubation. Thus 40 min was selected as the incubation time for the subsequent imaging experiments.

Cholinesterase (ChE) inhibitors, including 60 μmol L^{-1} tacrine (ChE

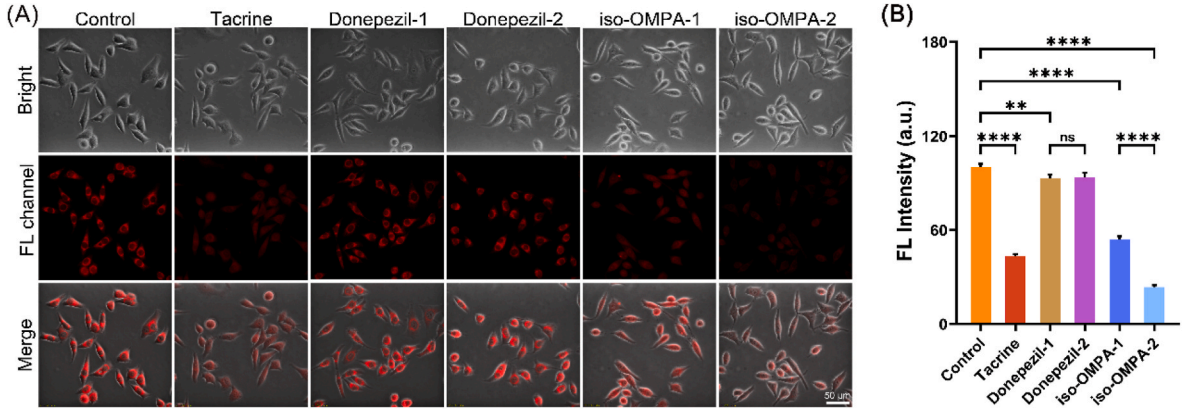

Fig. 5. Fluorescence images (A) and intensity (B) of HepG2 cells treated with tacrine (60 μmol L^{-1}), donepezil (30 and 60 μmol L^{-1}) and iso-OMPA (30 and 60 μmol L^{-1}). Scale bar, 50 μm. Incubation temperature, 37 °C; Excitation wavelength, 510–550 nm; Emission wavelength, >590 nm; ****$p < 0.0001$; ***$p < 0.001$; **$p < 0.01$.

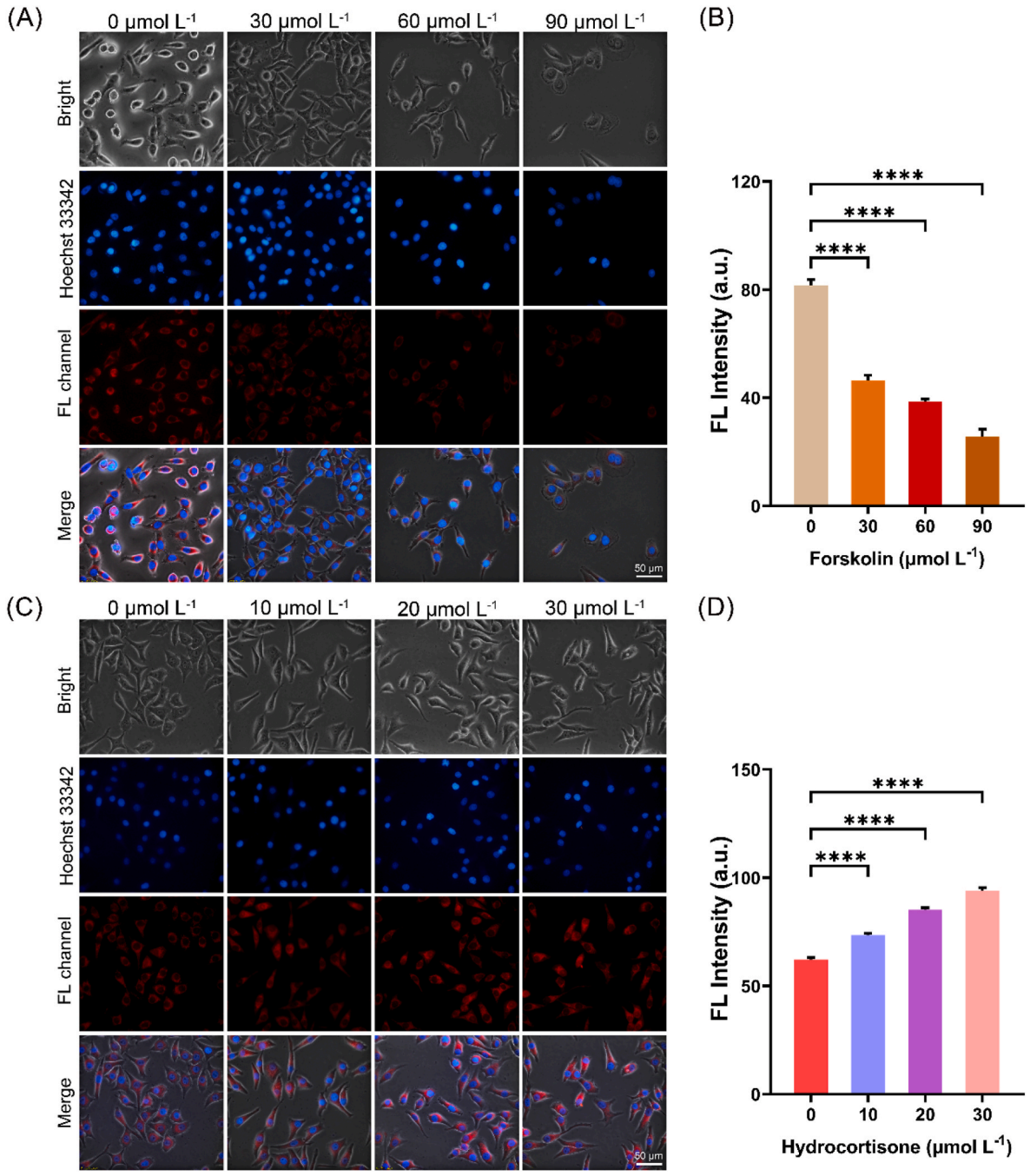

Fig. 6. Fluorescence images (A) and intensity (B) of HepG2 cells treated with different concentrations of forskolin (0, 30, 60 and 90 μmol L^{-1}). Fluorescence images (C) and intensity (D) of HepG2 cells treated with different concentrations of hydrocortisone (0, 10, 20 and 30 μmol L^{-1}). Scale bar, 50 μm. Incubation temperature, 37 °C; Excitation wavelength, 510–550 nm; Emission wavelength, >590 nm; ****$p < 0.0001$.

specific inhibitor), 30 and 60 μmol L^{-1} donepezil (AChE specific inhibitor) and 30 and 60 μmol L^{-1} iso-OMPA (BChE specific inhibitor), were incubated with HepG2 cells for 2 h, respectively. Afterwards the cells were incubated with 10 μmol L^{-1} HP-LZB for 40 min. The fluorescence images in Fig. 5 were collected after washing the cells with PBS buffer. The cells of the control group have strong red fluorescence, whereas the fluorescence of the cells treated with either tacrine or iso-OMPA turns significantly dark. However, the red fluorescence of cells treated with donepezil was still strong. These results indicate that HP-LZB has sensitive response to endogenous BChE but not to AChE and can specifically recognize BChE without interference from AChE in biological samples. Therefore the proposed probe can be useful for the screening of BChE inhibitors and for the further treatment of BChE-related diseases.

Forskolin is an activator of adenylate cyclase and was reported to down-regulate BChE expression in both human nerve and liver cancer cells [28,29]. A series concentrations of forskolin (30, 60 and 90 μmol L^{-1}) were incubated with HepG2 cells for 24 h. After that the cells were first incubated with Hoechst 33,342 and then with HP-LZB for 40 min before fluorescence imaging. As depicted in Fig. 6A, compared with the control group, the red fluorescence decreases with the increase of forskolin concentration in the medium. Thus an inverse relation between concentration of forskolin and the amount of intracellular BChE was observed, which is consistent with previous publications [28,29].

Hydrocortisone is an active form of glucocorticoid and may induce insulin resistance [28]. HepG2 cells were incubated in sequence with

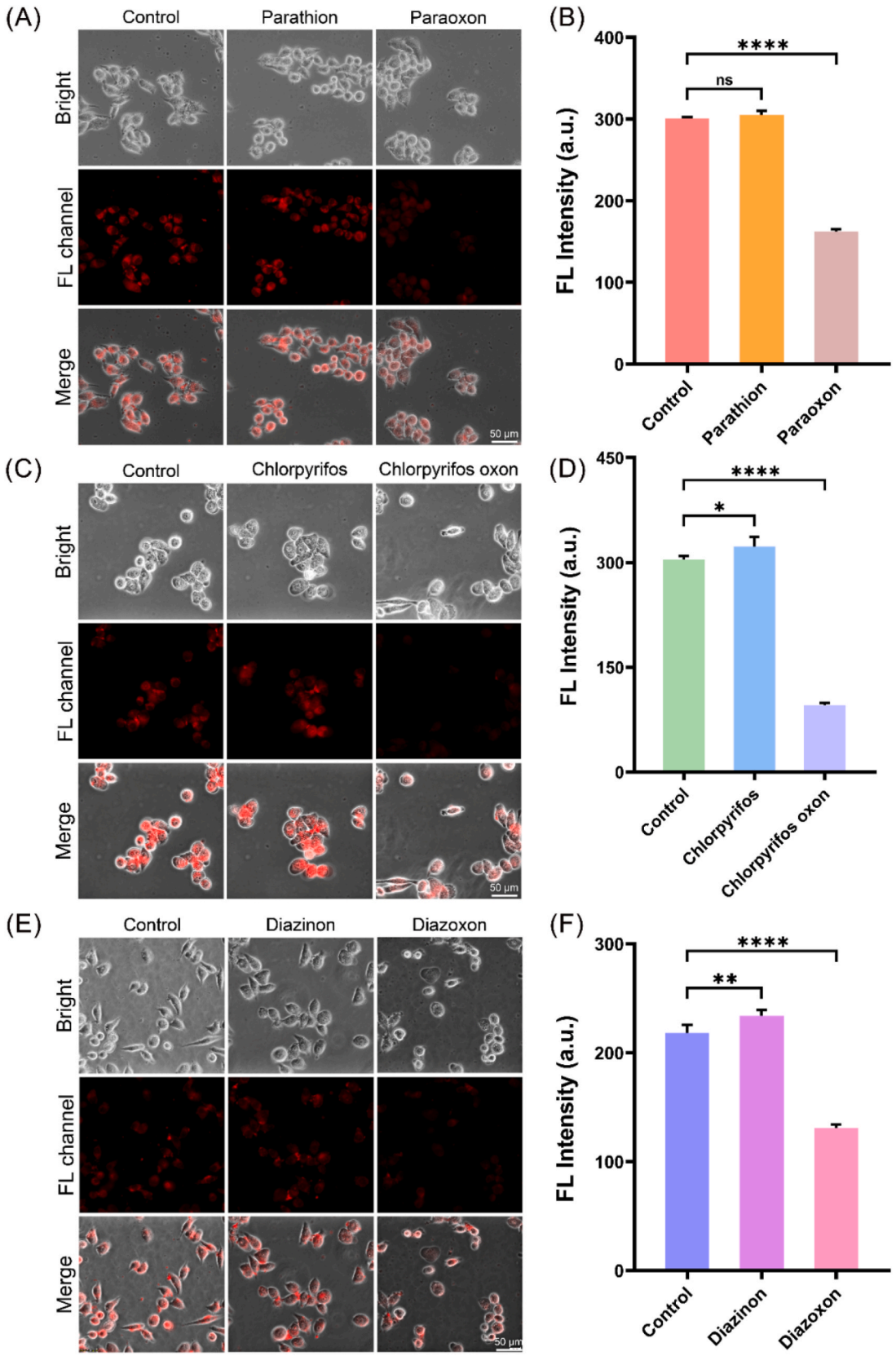

Fig. 7. Fluorescence images and intensity of HepG2 cells treated with thion and oxon OPs. Group 1: fluorescence image (A) and intensity (B) of parathion and paraoxon; Group 2: fluorescence image (C) and intensity (D) of chlorpyrifos and chlorpyrifos oxon; Group 3: fluorescence image (E) and intensity (F) of diazinon and diazoxon. Scale bar, 50 μm. Incubation temperature, 37 °C; Excitation wavelength, 510–550 nm; Emission wavelength, >590 nm; ****$p < 0.0001$; **$p < 0.01$; *$p < 0.1$.

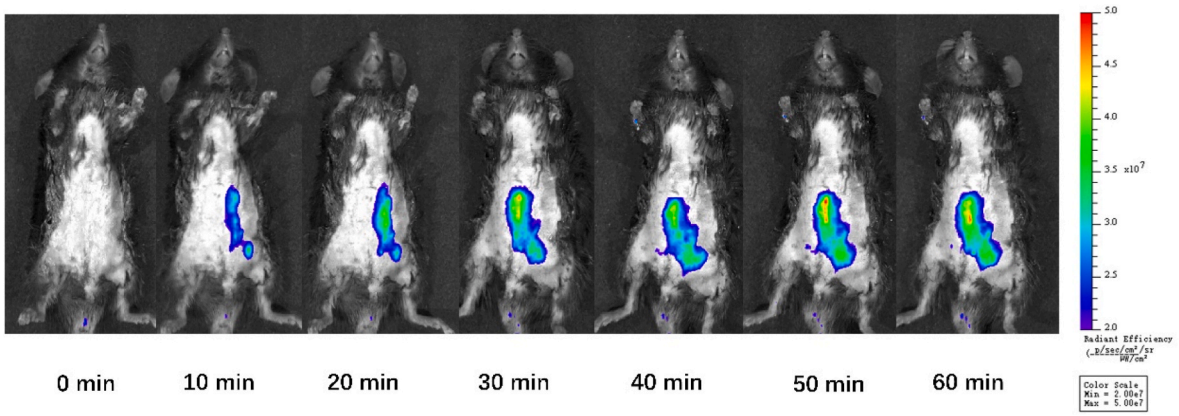

Fig. 8. Fluorescence images of the mouse after injection with 100 μL of 200 μmol L^{-1} HP-LZB.

hydrocortisone (10, 20 and 30 μmol L^{-1}), Hoechst 33,342 and HP-LZB before cellular imaging. As seen in Fig. 6C, the red fluorescent intensity of the cells increases with the increase of hydrocortisone concentration, indicating a proportional relation between concentration of hydrocortisone and BChE's level. The results are consistent with those obtained by Liu et al. with SH-SY5Y cells [28].

3.9. Visualization of interaction of oxon and thion OPs in living HepG2 cells

HepG2 cells in DMEM medium containing 10 % fetal bovine serum were cultured in 35 mm Petri dish at 37 °C for 24 h. Then the cells were incubated with 0.01 % Triton X-100 for 15–30 min in order to enhance the cell permeability. It has been demonstrated that a mild detergent treatment with very low concentration of Triton X-100 could preserve cell viability but increase the cell membrane permeability [30–32]. The cells were washed with PBS for three times for 2 min per wash. The experiments were divided into three groups according to the pesticide. In each group, there were 3 samples including control, thion pesticide and oxon pesticide. The pesticide concentration in each sample was 1.4 μg mL^{-1} and the incubation time was 10–20 min. After incubation with OPs, the pesticide was removed and HP-LZB was added at a concentration of 3 μmol L^{-1}. After 10 min, the cells were washed with PBS buffer and the fluorescence images in Fig. 7 were collected.

As seen in Fig. 7 within each group of the experiments, only oxon pesticide has effect on BChE. Compared with the control sample, the FL intensity of the cells decreases 46, 67 and 35 % after incubation with paraoxon, chlorpyrifos oxon and diazoxon, respectively. However, for three thion pesticides, there is no decrease in FL intensity, indicating that thion pesticide has no interaction with BChE and did not inhibit BChE's activity. These results are consistent with the in vitro data. In human or animal body, thion pesticide would be oxidized into its corresponding oxon molecule by enzyme cytochrome P450 (CYP450) mainly existent in liver [33,34]. However it was reported that HepG2 as the most widely used hepatoma cell line lacks expression of almost all human liver P450 enzymes and the activity of most P450 enzymes is undetectable in HepG2 cells [35]. Consequently, as in our results, thion pesticide was not oxidized into its oxon form and thus does not interact with BChE. Benefiting from our probe's excellent visualization capability for intercellular endogenous BChE, the interaction between BChE and either oxon or thion pesticide was intuitively and clearly observed by fluorescent microscope. In addition, the conversion and metabolism of thion pesticide in hepatoma cells could be explored visually.

3.10. In vivo imaging experiment

According to Fig. 8, the abdominal fluorescence appeared in the mouse model within 10 min after the injection of HP-LZB. With the prolongation of time from 10 to 30 min, the fluorescence area gradually expanded and the fluorescence intensity increased. Both fluorescence area and intensity reached an equilibrium level at 30 min after the injection of the probe. The results indicated that the probe HP-LZB was effective for visualizing BChE's level in the mouse model.

4. Conclusion

This work presents a novel near-infrared fluorescent probe for the evaluation of BChE's activity and detection of OPs both in vitro and in living hepatoma cells. The method is highly sensitive for the determination of oxon OPs. The chlorpyrifos oxon and diazoxon can be detected at very low LODs of 0.007 and 0.011 ng mL^{-1}, respectively. With very good anti-interference ability, the proposed fluorescent probe is prospective in the sensitive detection of OPs in real plant samples. Moreover, the off-on fluorescent probe with good visualization capability could be a promising tool for studying the metabolism of OPs and their interaction with cholinesterase in living cells.

CRediT authorship contribution statement

Zhimin Zhang: Writing – original draft, Validation, Investigation, Data curation, Conceptualization. **Jingkang Li:** Investigation, Data curation. **Bin Yang:** Investigation, Data curation. **Mo Ma:** Investigation. **Xiangdong Ding:** Investigation. **Hui Shi:** Formal analysis. **Pinyi Ma:** Formal analysis. **Daqian Song:** Supervision, Resources, Project administration. **Ziwei Zhang:** Writing – review & editing, Project administration, Data curation, Conceptualization.

Declaration of competing interest

The authors declare that they have no known competing financial interests or personal relationships that could have appeared to influence the work reported in this paper.

Data availability

Data will be made available on request.

Acknowledgments

The work was supported by Environmental Protection Research Project (No. 2024-17) of Jilin Provincial Department of Ecology and Environment.

Appendix A. Supplementary data

Supplementary data to this article can be found online at https://doi.

org/10.1016/j.talanta.2024.126587.

References

[1] H. Fu, P. Tan, R. Wang, S. Li, H. Liu, Y. Yang, Z. Wu, Advances in organophosphorus pesticides pollution: current status and challenges in ecotoxicological, sustainable agriculture, and degradation strategies, J. Hazard Mater. 424 (2022) 127494, https://doi.org/10.1016/j.jhazmat.2021.127494.

[2] S. Tanveer, N. Ilyas, N. Akhtar, N. Akhtar, N. Bostan, Z. Hasnain, A. Niaz, G. Zengin, A. Gafur, B. Fitriatin, Unlocking the interaction of organophosphorus pesticide residues with ecosystem: toxicity and bioremediation, Environ. Res. 249 (2024) 118291, https://doi.org/10.1016/j.envres.2024.118291.

[3] S.Y. Foong, N.L. Ma, S.S. Lam, W. Peng, F. Low, B.H.K. Lee, A.K.O. Alstrup, C. Sonne, A recent global review of hazardous chlorpyrifos pesticide in fruit and vegetables: prevalence, remediation and actions needed, J. Hazard Mater. 400 (2020) 123006, https://doi.org/10.1016/j.jhazmat.2020.123006.

[4] M. Wu, Y. Fan, J. Li, D. Lu, Y. Guo, L. Xie, Y. Wu, Vinyl phosphate-functionalized, magnetic, molecularly-imprinted polymeric microspheres' enrichment and carbon dots' fluorescence-detection of organophosphorus pesticide residues, Polymers 11 (2019) 1770, https://doi.org/10.3390/polym11111770.

[5] X. Wang, Y. Yang, Y. Yin, N. Zeng, Y. Dong, J. Liu, L. Wang, Z. Yang, C. Yang, High-throughput aptamer microarrays for fluorescent detection of multiple organophosphorus pesticides in food, Anal. Chem. 94 (2022) 3173–3179, https://doi.org/10.1021/acs.analchem.1c04650.

[6] L. Tang, C. Wang, S. Tian, Z. Zhang, Y. Yu, D. Song, Z. Zhang, Label-free and ultrasensitive detection of butyrylcholinesterase and organophosphorus pesticides by Mn(II)-Based electron spin resonance spectroscopy with a zero background signal, Anal. Chem. 94 (2022) 16189–16195, https://doi.org/10.1021/acs.analchem.2c03708.

[7] C. Padrón Sanz, R. Halko, Z. Sosa Ferrera, J.J. Santana Rodríguez, Micellar extraction of organophosphorus pesticides and their determination by liquid chromatography, Anal. Chim. Acta 524 (2004) 265–270, https://doi.org/10.1016/j.aca.2004.06.024.

[8] Z. Ma, Y. Gao, F. Chu, Y. Tong, Y. He, Y. Li, Z. Gao, W. Chen, S. Zhang, Y. Pan, Tip-assisted ambient electric arc ionization mass spectrometry for rapid detection of trace organophosphorus pesticides in strawberry, Chin. Chem. Lett. 33 (2022) 4411–4414, https://doi.org/10.1016/j.cclet.2021.12.029.

[9] I. Notardonato, E. Salimei, M.V. Russo, P. Avino, Simultaneous determination of organophosphorus pesticides and phthalates in baby food samples by ultrasound-vortex-assisted liquid-liquid microextraction and GC-IT/MS, Anal. Bioanal. Chem. 410 (2018) 3285–3296, https://doi.org/10.1007/s00216-018-0986-x.

[10] S. Luo, R. Peng, Y. Wang, X. Liu, J. Ren, W. Li, Y. Xiong, S. Yi, Q. Wen, Enzyme-targeted near-infrared fluorescent probe for organophosphorus pesticide residue detection, Anal. Bioanal. Chem. 415 (2023) 4849–4859, https://doi.org/10.1007/s00216-023-04801-9.

[11] C. Xiang, J. Xiang, X. Yang, C. Li, L. Zhou, D. Jiang, Y. Peng, Z. Xu, G. Deng, B. Zhu, P. Zhang, L. Cai, P. Gong, Ratiometric imaging of butyrylcholinesterase activity in mice with nonalcoholic fatty liver using an AIE-based fluorescent probe, J. Mater. Chem. B 10 (2022) 4254–4260, https://doi.org/10.1039/D2TB00422D.

[12] N. Nechaeva, T. Prokopkina, G. Makhaeva, E. Rudakova, N. Boltneva, C. Dishovsky, A. Eremenko, I. Kurochkin, Quantitative butyrylcholinesterase activity detection by surface-enhanced Raman spectroscopy, Sensor. Actuator. B Chem. 259 (2018) 75–82, https://doi.org/10.1016/j.snb.2017.11.174.

[13] A. Acari, T. Almammadov, M. Dirak, G. Gulsoy, S. Kolemen, Real-time visualization of butyrylcholinesterase activity using a highly selective and sensitive chemiluminescent probe, J. Mater. Chem. B 11 (2013) 6881–6888, https://doi.org/10.1039/D3TB01022H.

[14] R. Zhai, G. Chen, G. Liu, X. Huang, X. Xu, L. Li, Y. Zhang, J. Wang, M. Jin, D. Xu, A. El-Aty, Enzyme inhibition methods based on Au nanomaterials for rapid detection of organophosphorus pesticides in agricultural and environmental samples: a review, J. Adv. Res. 37 (2022) 61–74, https://doi.org/10.1016/j.jare.2021.08.008.

[15] C.S. Pundir, A. Malik, Preety. Bio-sensing of organophosphorus pesticides: a review, Biosens. Bioelectron. 140 (2019) 111348, https://doi.org/10.1016/j.bios.2019.111348.

[16] W. Yuan, C. Wan, J. Zhang, Q. Li, P. Zhang, K. Zheng, Q. Zhang, C. Ding, Near-infrared ratiometric fluorescent strategy for butyrylcholinesterase activity and its application in the detection of pesticide residue in food samples and biological imaging, Spectrochim. Acta Mol. Biomol. Spectrosc. 297 (2023) 122719, https://doi.org/10.1016/j.saa.2023.122719.

[17] Q. Zhang, C. Fu, X. Guo, J. Gao, P. Zhang, C. Ding, Fluorescent determination of butyrylcholinesterase activity and its application in biological imaging and pesticide residue detection, ACS Sens. 6 (2021) 1138–1146, https://doi.org/10.1021/acssensors.0c02398.

[18] B. Yang, X. Ding, Z. Zhang, J. Li, S. Fan, J. Lai, R. Su, X. Wang, B. Wang, Visualization of production and remediation of acetaminophen-induced liver injury by a carboxylesterase-2 enzyme-activatable near-infrared fluorescent probe, Talanta 269 (2024) 125418, https://doi.org/10.1016/j.talanta.2023.125418.

[19] S. Yang, Q. Sun, H. Xiong, S. Liu, B. Moosavi, W. Yang, G. Yang, Discovery of a butyrylcholinesterase-specific probe via a structure-based design strategy, Chem. Commun. 53 (2017) 3952–3955, https://doi.org/10.1039/C7CC00577F.

[20] M. Dirak, J.F.R. Chan, S. Kolemen, Optical imaging probes for selective detection of butyrylcholinesterase, J. Mater. Chem. B 12 (2024) 1149–1167, https://doi.org/10.1039/D3TB02468G.

[21] R. Wang, F. Zhang, NIR luminescent nanomaterials for biomedical imaging, J. Mater. Chem. B 2 (2014) 2422–2443, https://doi.org/10.1039/C3TB21447H.

[22] T. Ren, W. Xu, W. Zhang, X. Zhang, Z. Wang, Z. Xiang, L. Yuan, X. Zhang, A general method to increase Stokes shift by introducing alternating vibronic structures, J. Am. Chem. Soc. 140 (2018) 7716–7722, https://doi.org/10.1021/jacs.8b04404.

[23] L. Xu, M. Ma, J. Li, H. Yang, D. Gao, P. Ma, D. Song, Exploring butyrylcholinesterase expression in diseases using a promising fluorescent imaging tool, Sensor. Actuator. B Chem. 394 (2023) 134432, https://doi.org/10.1016/j.snb.2023.134432.

[24] S.O. Obare, C. De, W. Guo, T.L. Haywood, T.A. Samuels, C.P. Adams, N.O. Masika, D.H. Murray, G.A. Anderson, K. Campbell, K. Fletcher, Fluorescent chemosensors for toxic organophosphorus pesticides: a review, Sensors 10 (2010) 7018–7043, https://doi.org/10.3390/s100707018.

[25] D.W. Sparling, G. Fellers, Comparative toxicity of chlorpyrifos, diazinon, malathion and their oxon derivatives to larval Rana boylii, Environ. Pollut. 147 (2007) 535–539, https://doi.org/10.1016/j.envpol.2006.10.036.

[26] A.P. Kulkarni, E. Hodgson, Metabolism of insecticides by mixed function oxidase systems, Pharmacol. Ther. 8 (1980) 379–475, https://doi.org/10.1016/0163-7258(80)90054-6.

[27] K.S. Law, R.A. Acey, C.R. Smith, D.A. Benton, S. Soroushian, B. Eckenrod, R. Stedman, K.A. Kantardjieff, K. Nakayama, Dialkyl phenyl phosphates as novel selective inhibitors of butyrylcholinesterase, Biochem. Biophys. Res. Commun. 355 (2007) 371–378, https://doi.org/10.1016/j.bbrc.2007.01.186.

[28] S. Liu, H. Xiong, J. Yang, S. Yang, Y. Li, W. Yang, G. Yang, Discovery of butyrylcholinesterase-activated near-infrared fluorogenic probe for live-cell and in vivo imaging, ACS Sens. 3 (2018) 2118–2128, https://doi.org/10.1021/acssensors.8b00697.

[29] Y. Yang, L. Zhang, J. Wang, Y. Cao, S. Li, W. Qin, Y. Liu, Diagnosis of alzheimer's disease and in situ biological imaging via an activatable near-infrared fluorescence probe, Anal. Chem. 94 (2022) 13498–13506, https://doi.org/10.1021/acs.analchem.2c02627.

[30] S.P. Samuel, N. Jain, F. O'Dowd, T. Paul, D. Kashanin, V.A. Gerard, Y.K. Gun'ko, A. Prina-Mello, Y. Volkov, Multifactorial determinants that govern nanoparticle uptake by human endothelial cells under flow, Int. J. Nanomed. 7 (2012) 2943–2956, https://doi.org/10.2147/IJN.S30624.

[31] Y. Williams, A. Sukhanova, M. Nowostawska, A.M. Davies, S. Mitchell, V. Oleinikov, Y. Gun'ko, I. Nabiev, D. Kelleher, Y. Volkov, Probing cell-type-specific intracellular nanoscale barriers using size-tuned quantum dots, Small 5 (2009) 2581–2588, https://doi.org/10.1002/smll.200900744.

[32] A.L. van de Ven, K. Adler-Storthz, R. Richards-Kortum, Delivery of optical contrast agents using Triton-X100, part 1: reversible permeabilization of live cells for intracellular labeling, J. Biomed. Opt. 14 (2009) 021012, https://doi.org/10.1117/1.3090448.

[33] E.G. Duysen, J.R. Cashman, L.M. Schopfer, F. Nachon, P. Masson, O. Lockridge, Differential sensitivity of plasma carboxylesterase-null mice to parathion, chlorpyrifos and chlorpyrifos oxon, but not to diazinon, dichlorvos, diisopropylfluorophosphate, cresyl saligenin phosphate, cyclosarin thiocholine, tabun thiocholine, and carbofuran, Chem. Biol. Interact. 195 (2012) 189–198, https://doi.org/10.1016/j.cbi.2011.12.006.

[34] I. Hreljac, I. Zajc, T. Lah, M. Filipic, Effects of model organophosphorous pesticides on DNA damage and proliferation of HepG2 cells, Environ. Mol. Mutagen. 49 (2008) 360–367, https://doi.org/10.1002/em.20392.

[35] M.T. Donato, A. Lahoz, J.V. Castell, M.J. Gómez-Lechón, Cell lines: a tool for in vitro drug metabolism studies, Curr. Drug Metabol. 9 (2008) 1–11, https://doi.org/10.2174/138920008783331086.